Geometry Selection of a Redundantly Actuated Cable-Suspended Parallel Robot

Marc Gouttefarde, *Member, IEEE*, Jean-François Collard, Nicolas Riehl, and Cédric Baradat

***Abstract*—This paper is dedicated to the geometry selection of a redundantly actuated cable-suspended parallel robot intended to manipulate heavy payloads over a wide workspace. Cable-suspended refers here to cable-driven parallel robots in a crane-like setting, where all the cable drawing points are located on top of the base frame, gravity being used to keep the cables taut. Geometry selection consists of determining the relative positions of the cable drawing points on the base frame and of the cable attachment points on the mobile platform together with the cable arrangement between these two sets of points. An original performance index is introduced. It is defined as the maximum acceptable distance between the mobile platform geometric center and the center of mass of the set consisting of the platform and a payload. This performance index is of particular interest in heavy payload handling applications. Used within a two-phase geometry selection strategy, it yields a new cable-suspended robot geometry having a very large workspace to footprint ratio and able to handle heavy payloads. A large-dimension redundantly actuated cable-suspended robot was built in order to demonstrate these capabilities.**

***Index Terms*—Cable-driven parallel robots, kinematics, parallel robots.**

I. Introduction

This paper deals with *cable-suspended parallel robots*. As illustrated in Fig. 1, this name refers here to cable-driven parallel robots, whose cable drawing points are all located above the mobile platform. A well-known 6-degree-of-freedom (DOF) cable-suspended robot is the NIST ROBOCRANE [1]. As opposed to fully constrained cable-driven parallel robots such as the FALCON [2], the weight of the mobile platform (and payload) is necessary to keep the cables taut. The part of the workspace located below the mobile platform is free of cables, making this type of cable robot attractive for applications like heavy payload handling. In this study, we focus on 6-DOF redundantly actuated cable-suspended robots, and hence, we do not consider underconstrained robots [3], which are driven by less cables than DOF. Additionally, unlike in [4] and [5], the cable drawing points are supposed to be fixed (no mobile bases).

The mobile platform of a cable-driven parallel robot is connected to winches by means of a set of cables. The cables are attached to the mobile platform, and exit from the robot fixed base at some points, referred to as the cable drawing points. The relative positions in space of the cable drawing points define the *base geometry*. We define the *platform geometry* as the relative positions of the cable attachment points on the mobile platform. Moreover, a *cable-driven parallel robot geometry* is defined as the set consisting of the base geometry, the mobile platform geometry, and the cable connections (or arrangement) between them.

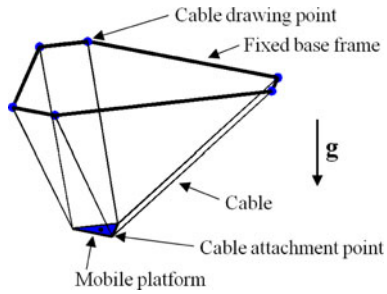

Fig. 1. Sketch of a cable-suspended parallel robot.

The selection of a cable-driven parallel robot geometry is a fundamental choice because it strongly influences the robot performances. Most of the previous works dealing with geometry selection are dedicated to fully constrained cable-driven parallel robots. In several papers [2], [6]–[11], the geometry selection process itself is either not discussed or not the result of a systematic methodology. On the contrary, the use of various optimization techniques are presented in [4], [5], and [12]–[15]. The main criteria is the wrench-closure workspace, or other types of wrench-feasible workspaces [16], and avoidance of cable collisions. An initial geometry is generally limited to start the optimization process making the exploration of the design space usually limited. Other fully constrained cable robot geometries were obtained by means of geometric or other *ad hoc* considerations [17], [18]. The early work by Tadokoro *et al.* [19] is an exception. Indeed, unlike in the aforementioned papers, the combinatorial nature of the possible cable connections between some given base and platform geometries is explicitly considered. It enables a much wider variety of fully constrained cable robot geometries to be explored. Recently, in the context of the synthesis of differential cable-driven parallel robots, all possible arrangements of cable segments in a differential were studied in [20].

The geometry selection of cable-suspended robots has been less discussed than that of fully constrained robots. In [1], the geometry of the NIST ROBOCRANE is introduced as an upside-down Gough–Stewart platform with triangular base and platform. The influences of some geometric parameters on the static

Manuscript received April 8, 2014; revised December 4, 2014; accepted January 29, 2015. Date of publication February 26, 2015; date of current version April 2, 2015. This paper was recommended for publication by Associate Editor V. Krovi and Editor C. Torras upon evaluation of the reviewers' comments. This work was supported by the ANR under Grant 2009 SEGI 018, Project CoGiRo, and by the Région Languedoc-Roussillon under Grant 140218.

M. Gouttefarde is with Laboratoire d'Informatique, de Robotique et de Microélectronique de Montpellier, CNRS-Université Montpellier 2, 34095 Montpellier Cedex 5, France (e-mail: marc.gouttefarde@lirmm.fr).

J.-F. Collard is with the Center for Research in Mechatronics, Université catholique de Louvain 1348, Louvain-la-Neuve, Belgium (e-mail: jf.collard@uclouvain.be).

N. Riehl and C. Baradat are with TECNALIA France, 34000 Montpellier Cedex 2, France (e-mail: nriehl@gmail.com; cedric.baradat@tecnalia.com).

Color versions of one or more of the figures in this paper are available online at http://ieeexplore.ieee.org.

Digital Object Identifier 10.1109/TRO.2015.2400253

workspace and on the global condition index of such 6-6 cable-suspended parallel robots are studied in [21]. The dimensional design of the 6-cable-suspended parallel manipulator of FAST is reported in [22]. A less conventional 6-cable-suspended robot geometry is presented in [23] for a particular application. In all these works, a limited number of geometric parameters is considered, and all possible cable connections are not explicitly studied. Consequently, the set of investigated cable-suspended robot geometries is not very large.

None of the aforementioned previous works deals with the geometry selection of redundantly actuated cable-suspended parallel robots, which is the topic of this study. A two-phase geometry selection methodology is considered. Inspired by Tadokoro *et al.*[19], the first phase of this methodology consists of testing a very large number of possible cable connections between various base and platform preselected geometries. The second phase aims at refining the result of the first phase using standard gradient-based optimization. While this two-stage methodology is not particularly novel, the result of its application to redundantly actuated cable-suspended parallel robots is the main contribution of this paper. Indeed, it yields a *new cable-suspended robot geometry* having a very large workspace to footprint ratio and able to manipulate heavy payloads. To demonstrate these capabilities, a large-dimension 8-cable 6-DOF robot was built in the framework of a research project called CoGiRo.

The second contribution of this paper is a particular wrench-feasibility analysis. A mobile platform pose is said to be wrench-feasible when a required wrench set (RW) is entirely contained within the set of wrenches that the cables are able to apply, called the available wrench set (AW) [24]. The particularity of the analysis proposed in this paper lies in the definition of the RW. In previous works, e.g., [24]–[27], this set is a hyperellipsoid, a hyperrectangle, or it is reduced to a unique wrench. Focusing on heavy payload handling tasks, the RW introduced in this study corresponds to the wrenches that permit to balance the total weight of the platform and the payload. When both the mass and the center of mass (CoM) position are variable, this RW is a truncated cone. The analysis of the conditions under which this cone is completely contained within the AW leads us to a *new performance index* defined as the maximum acceptable horizontal distance between the mobile platform geometric center and the CoM of the set consisting of the platform and the payload. This index is of particular interest in applications involving heavy payload manipulations.

This paper is organized as follows. The particular wrench-feasibility analysis and the resulting new performance index are introduced in Section II. The two-phase geometry selection methodology is summarized in Section III. The application of this methodology to the geometry selection of a 6-DOF cable-suspended parallel robot driven by eight cables is presented in Section IV.

II. Wrench-Feasibility Analysis

In this paper, the evaluation of cable-suspended parallel robot geometries relies on their quasi-static behavior. Compared with the static ones, the forces and moments due to the mobile platform dynamics are neglected. Our goal is to evaluate the ability to handle payloads that may not be centered with respect to (w.r.t.) the platform reference point. To this end, we introduce an original performance index defined as the *maximum acceptable horizontal distance between the platform reference point and the CoM of the set composed of the platform and a payload*. Sections II-A and II-B present the usual static equilibrium equations and wrench-feasibility analysis, respectively. Section II-C introduces the particular RW considered in this paper. Finally, Section II-D shows how the aforementioned original performance index can be computed.

A. Static Modeling of Cable-Suspended Parallel Robots

Neglecting the mass of the cables, the static equilibrium of a 6-DOF cable-driven parallel robot mobile platform is given by Hiller *et al.* [9] and Roberts *et al.* [28] as

$$\mathbf{W}\,\boldsymbol{\tau} + \mathbf{f}_e = \mathbf{0} \tag{1}$$

where $\mathbf{W}$ is the so-called wrench matrix of dimension $6 \times n$, n denotes the number of cables ($n \geq 6$ in this paper), $\boldsymbol{\tau}$ is the column vector containing the cable tensions, and $\mathbf{f}_e$ is the external wrench applied to the platform at its reference point.

Cable tensions are subjected to minimal and maximal admissible values. The maximal value $\tau_{\max}$ is necessary in order to take into account mechanical limits (e.g., cable breaking load or force sensor maximum load). The minimal value $\tau_{\min}$ must be nonnegative because the cables cannot push on the mobile platform. For cable-suspended parallel robots, since the cables are not acting antagonistically on the mobile platform, the minimal tension $\tau_{\min}$ should be set to a small value or to zero.

B. Wrench-Feasibility Analysis

Following the analysis proposed in [24], for a given pose (position and orientation) of the platform, the AW is defined as the set of wrenches $\mathbf{f}$ that the cables *can* generate at the mobile platform reference point

$$\mathrm{AW} = \{\mathbf{f} = \mathbf{W}\,\boldsymbol{\tau} \;\mid\; \boldsymbol{\tau}_{\min} \leq \boldsymbol{\tau} \leq \boldsymbol{\tau}_{\max}\} \tag{2}$$

where the components of the n-dimensional vector $\boldsymbol{\tau}_{\min}$ are all equal to the minimal admissible cable tension $\tau_{\min} \geq 0$, and all the components of $\boldsymbol{\tau}_{\max}$ are equal to $\tau_{\max}$. Besides, the RW is the set of wrenches that the cables *must* exert on the platform to complete a task. The exact definition of the RW is directly related to the application or task(s) at hand. A mobile platform pose is said to be *wrench-feasible* when RW $\subseteq$ AW, which means that the cables can generate any wrench in RW while satisfying the constraints $\boldsymbol{\tau}_{\min} \leq \boldsymbol{\tau} \leq \boldsymbol{\tau}_{\max}$.

Even for geometrically simple RW, testing wrench feasibility by means of (2) is generally an issue. However, being the image of the hypercube $\boldsymbol{\tau}_{\min} \leq \boldsymbol{\tau} \leq \boldsymbol{\tau}_{\max}$ under the linear map represented by matrix $\mathbf{W}$, AW is a convex polytope and can, thus, be represented as the solution set of a system of linear inequalities [29]

$$\mathrm{AW} = \{\mathbf{f} \;\mid\; \mathbf{C}\mathbf{f} \leq \mathbf{d}\}\,. \tag{3}$$

Testing wrench feasibility by means of (3) is generally straightforward. For example, when RW is defined as a hypercube, RW $\subseteq$ AW if and only if all hypercube vertices $\mathbf{f}_v$ satisfy $\mathbf{C}\mathbf{f}_v \leq \mathbf{d}$. The difficulty lies in the determination of matrix $\mathbf{C}$ and vector $\mathbf{d}$. They can be obtained efficiently by means of the so-called hyperplane shifting method introduced in [25]. Let us briefly present this method being given that a comprehensive description can be found in [25] and [30].

For a $6 \times n$ wrench matrix $\mathbf{W}$ (6-DOF and $n \geq 6$ cables), each combination of five *linearly independent* columns $\mathbf{w}_{i_1}, \ldots, \mathbf{w}_{i_5}$ of $\mathbf{W}$ provides two lines of $\mathbf{C}$, say $\mathbf{c}_k^T$ and $\mathbf{c}_l^T$. The line $\mathbf{c}_k^T$ is given by $\mathbf{c}_k = \mathbf{c}_I = \text{null}\,(\mathbf{M}_I)$, where $\mathbf{c}_I = \text{null}\,(\mathbf{M}_I)$ denotes a vector spanning the nullspace of the 5×6 matrix

$$\mathbf{M}_I = [\mathbf{w}_{i_1},\ \mathbf{w}_{i_2}, \ldots,\ \mathbf{w}_{i_5}]^T \tag{4}$$

and I denotes the index set $\{i_1, \ldots, i_5\} \subset \{1, \ldots, n\}$. The other line is $\mathbf{c}_l^T = -\mathbf{c}_I^T$. The total number N_h of lines of matrix $\mathbf{C}$ is equal to twice the number of possible combinations of five *linearly independent* columns of the wrench matrix $\mathbf{W}$.

Complementing the work done in [25], it was shown in [30] that the two elements d_k and d_l of vector $\mathbf{d}$ corresponding to the lines $\mathbf{c}_k^T$ and $\mathbf{c}_l^T$ of matrix $\mathbf{C}$ are given by

$$d_k = \sum_{i \in I^+} \tau_{\max} \mathbf{c}_I^T \mathbf{w}_i + \sum_{i \in I^-} \tau_{\min} \mathbf{c}_I^T \mathbf{w}_i \tag{5}$$

$$d_l = -\sum_{i \in I^-} \tau_{\max} \mathbf{c}_I^T \mathbf{w}_i - \sum_{i \in I^+} \tau_{\min} \mathbf{c}_I^T \mathbf{w}_i \tag{6}$$

where I^+ and I^- are the subsets of $\{1, \ldots, n\}$ defined as

$$I^+ = \left\{ i \mid \mathbf{c}_I^T \mathbf{w}_i > 0 \right\} \text{ and } I^- = \left\{ i \mid \mathbf{c}_I^T \mathbf{w}_i < 0 \right\}. \tag{7}$$

In the sequel, the line $\mathbf{c}_j^T$ of matrix $\mathbf{C}$ is denoted as follows:

$$\mathbf{c}_j^T = \left[c_{j_{f_x}}\ c_{j_{f_y}}\ c_{j_{f_z}}\ c_{j_{t_x}}\ c_{j_{t_y}}\ c_{j_{t_z}} \right] \tag{8}$$

where $f_x, f_y, \ldots, t_z$ stand for the force and moment components of a wrench $\mathbf{f} = [f_x, f_y, f_z, t_x, t_y, t_z]^T$.

C. Required Wrench Set

The originality of the wrench-feasibility analysis conducted in this paper comes mainly from the RW introduced in this section. This RW is the wrench set that the cables must apply to the mobile platform in order to balance the platform and payload weight for a set of possible masses and positions of the CoM. This RW is notably relevant in cable-driven parallel robot applications involving the manipulation of heavy payloads of various sizes and weights. Indeed, in such applications, the CoM of the set composed of the robot mobile platform and a payload is generally not coincident with the mobile platform reference point P and its position can change from one payload to another.

In the sequel, we refer to the platform reference point P as the platform *geometric center*. The CoM of the set consisting of the mobile platform and a payload is denoted by C. For a given platform orientation, as illustrated in Fig. 2, C is usually not located on the vertical line passing through point P. The (horizontal) distance between C and this vertical line is denoted by h. The sum of the platform and payload masses is denoted by m, whereas $g = 9.81\ \text{ms}^{-2}$ is the gravity acceleration. In a frame having a vertical z-axis and whose origin is the platform geometric center P, e.g., the frame (P, X', Y', Z') shown in Fig. 2, the wrench $\mathbf{f} = [f_x, f_y, f_z, t_x, t_y, t_z]^T$ that the cables must apply to balance the platform and payload weights is

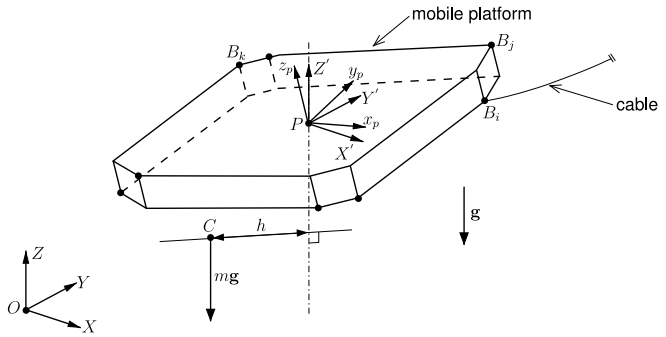

Fig. 2. Cable-suspended parallel robot mobile platform—Points B_i are the cable attachment points, P is the platform reference point ("geometric center"), and C is the platform and payload CoM. The reference frame (O, X, Y, Z) is fixed, and its axis Z is vertical. (P, x_p, y_p, z_p) is a local frame attached to the platform. The frame (P, X', Y', Z') is centered at P, but it has the same orientation as the fixed reference frame, i.e., $X' = X$, $Y' = Y$, and $Z' = Z$. Axis Z' is, thus, vertical.

$$f_x = f_y = t_z = 0,\ f_z = mg \text{ and } \sqrt{t_x^2 + t_y^2} = mgh \tag{9}$$

where f_x, f_y, and f_z are forces along the X', Y', and Z' axes, respectively, and t_x, t_y, and t_z are moments about these axes. Only the horizontal distance h is relevant, since $\mathbf{f}$ is not influenced by the vertical position of the CoM C. Note that for a given position of C in the local platform frame, the distance h depends on the platform orientation, i.e., on the angle between z_p and the vertical axis.

Let us consider that the position of C and the mass m are not exactly known and/or subjected to changes in such a way that $0 \leq h \leq r$ and $m_{\min} \leq m \leq m_{\max}$, where r, $m_{\min}$, and $m_{\max}$ are positive scalars. Typically, $m_{\min}$ is the mass of the empty mobile platform, and $m_{\max}$ is the sum of the platform and heaviest payload masses. Such a situation leads to a set of possible wrenches at point P that the cables must be able to apply to the set platform-payload to balance their total weight. This wrench set is the RW considered in this paper. It is defined as

$$\begin{aligned} \text{RW} = \{ \mathbf{f} \mid\ & f_x = f_y = t_z = 0,\ m_{\min} g \leq f_z \leq m_{\max} g \\ & 0 \leq \sqrt{t_x^2 + t_y^2} \leq mgr \}. \end{aligned} \tag{10}$$

In the space of wrenches applied by the cables at the platform geometric center P, this RW is a truncated cone embedded in the 3-D subspace $f_x = f_y = t_z = 0$, as shown in Fig. 3. It is apparent in the figure, and is not difficult to prove that this RW

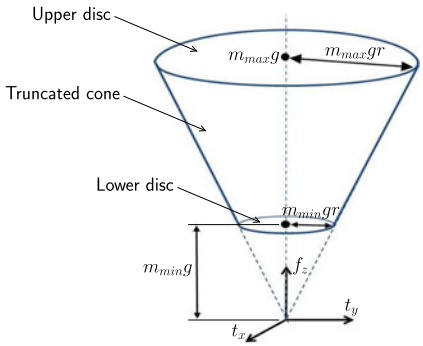

Fig. 3. RW considered in this paper: A truncated cone.

is the convex hull of its lower disc $\mathcal{L}$ and upper disc $\mathcal{U}$, where

$$\mathcal{L} = \{\mathbf{f} \mid f_x = f_y = t_z = 0,\ f_z = m_{\min} g \\ 0 \le \sqrt{t_x^2 + t_y^2} \le m_{\min} g r\} \quad (11)$$

$$\mathcal{U} = \{\mathbf{f} \mid f_x = f_y = t_z = 0,\ f_z = m_{\max} g \\ 0 \le \sqrt{t_x^2 + t_y^2} \le m_{\max} g r\}. \quad (12)$$

The AW being also a convex set, a given mobile platform pose is wrench-feasible, i.e., RW $\subseteq$ AW, if and only if both the lower disc $\mathcal{L}$ and the upper disc $\mathcal{U}$ of RW are entirely contained within AW.

D. Performance Index Definition

In this paper, we are interested in the maximum value $r_{\max}$ of r such that RW defined in (10) is fully included in AW. For a platform and payload total mass comprised between $m_{\min}$ and $m_{\max}$, $r_{\max}$ corresponds to the *maximum acceptable horizontal distance* between the platform geometric center P and the CoM C. According to the definition of AW, admissible means that each cable tension lies in the nonnegative interval $[\tau_{\min}, \tau_{\max}]$. For a given pose of the mobile platform, $r_{\max}$ indicates to which extent the CoM can be shifted w.r.t. the platform reference point P while keeping admissible cable tensions. It will be used in Section III as a performance index to evaluate and optimize cable-suspended parallel robot geometries.

Referring to Section II-C, RW $\subseteq$ AW if and only if both the lower disc $\mathcal{L}$ and the upper disc $\mathcal{U}$ of RW are entirely contained in AW. Consequently, $r_{\max}$ is the largest value of r such that both $\mathcal{L}$ and $\mathcal{U}$ are fully included in AW. Let us first consider the case of the upper disc $\mathcal{U}$. As proved in the appendix, the maximum value r_1 of r such that $\mathcal{U}$ is fully included in AW is equal to

$$r_1 = \min_j r_{1,j} = \min_j \frac{\frac{d_j}{m_{\max} g} - c_{j_{f_z}}}{\sqrt{c_{j_{t_x}}^2 + c_{j_{t_y}}^2}}. \quad (13)$$

The case of the lower disc $\mathcal{L}$ is similar to the case of the upper disc but with $m_{\min}$ in place of $m_{\max}$, i.e., the maximum value

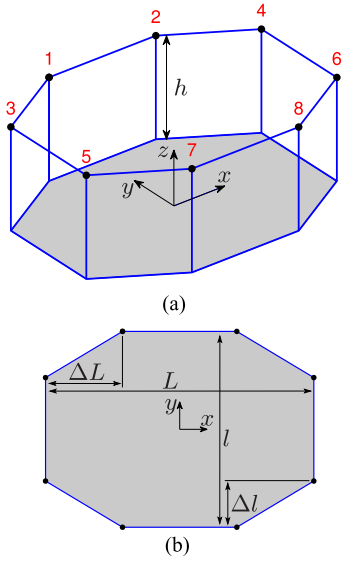

Fig. 4. Base geometry type parameterized by L, l, h, ΔL, and Δl. (a) 3-D view. (b) 2-D top view.

r_2 of r such that $\mathcal{L}$ is fully included in AW is equal to

$$r_2 = \min_j r_{2,j} = \min_j \frac{\frac{d_j}{m_{\min} g} - c_{j_{f_z}}}{\sqrt{c_{j_{t_x}}^2 + c_{j_{t_y}}^2}}. \quad (14)$$

Therefore, for a given pose of the platform, the maximum acceptable horizontal distance between the platform geometric center P and the platform and payload CoM C, i.e., the largest value of r such that RW $\subseteq$ AW, is given by

$$r_{\max} = \min_{i=1,2} r_i = \min_{i,j} r_{i,j} \quad (15)$$

with

$$r_{i,j} = \frac{\frac{d_j}{m_i g} - c_{j_{f_z}}}{\sqrt{c_{j_{t_x}}^2 + c_{j_{t_y}}^2}},\ i = 1, 2, \text{ and } j = 1, \ldots, N_h \quad (16)$$

where $m_1 = m_{\max}$ and $m_2 = m_{\min}$.

III. Optimal Geometry Selection Methodology

A. Phase 1: Exploration

The first phase of the geometry selection methodology used in this paper consists of generating and testing a discrete, but large number of possible cable-driven parallel robot geometries. In contrast with a local optimization, this first phase aims to explore "globally" the very wide space of possible robot geometries in order to find a good starting point for the optimization performed in the second phase (see Section III-B). To this end, a strategy divided into four subsequent steps is summarized in this section.

1) Step 1 (User-Defined Parameters): The number of mobile platform DOF and the number of cables are first defined. In this paper, 6-DOF parallel robots driven by $n = 8$ cables are considered. The user also defines a number of base and platform *geometry types*. A base (resp. platform) geometry type is defined as a set of *distinct points* at which the cables exit from the

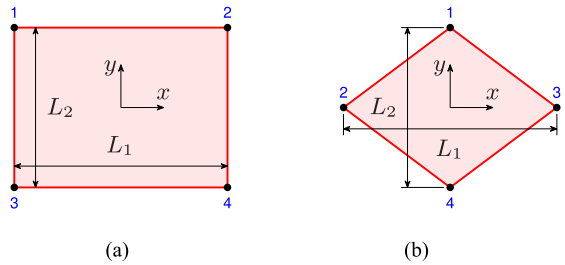

Fig. 5. Two four-point platform geometry types parameterized by L_1 and L_2. (a) Rectangular platform. (b) Diamond platform.

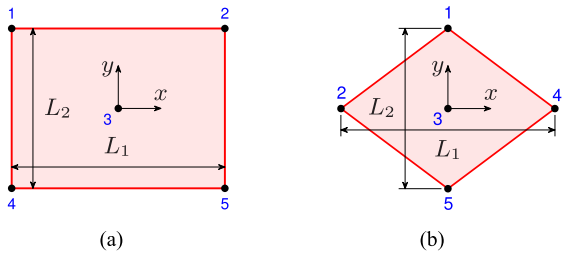

Fig. 6. Two five-point platform geometry types parameterized by L_1 and L_2. (a) Rectangular platform. (b) Diamond platform.

fixed base (resp. are attached to the mobile platform) and a set of dimensional parameters defining the relative positions between these distinct points. For instance, in Fig. 5(a), four distinct cable attachment points define a rectangular mobile platform geometry type whose dimensional parameters are the edge lengths L_1 and L_2. For each dimensional parameter of the base and platform geometry types, a discrete set of possible values is defined by the user.

A base (resp. platform) geometry is fully specified by a base (resp. platform) geometry type together with particular values assigned to each of its dimensional parameters. These values are taken among the discrete set of possible ones.

The base and platform geometry types may have some symmetry properties, in which the corresponding symmetry rules are also specified. In many applications, the prescribed workspace is symmetric. Moreover, symmetric cable-driven parallel robot geometries should possess more homogeneous performances across their workspace. In this paper, each point of a geometry type has a symmetric point w.r.t. the z-axis, i.e., points having coordinates (x, y, z) and $(-x, -y, z)$ are symmetrical to each other. Note that the z-axis of the local frame attached to the mobile platform is vertical when the platform lies in its reference orientation. Symmetries w.r.t. this z-axis are considered because we are dealing with cable-suspended parallel robots which rely on gravity to keep the cables in tension.

Additionally, a prescribed workspace is defined together with a discrete set of poses defining a discretization of this workspace. Other necessary modeling and performance criterion related parameters are finally to be specified. In this paper, only the minimum and maximum mass values $m_{\min}$ and $m_{\max}$ need to be defined.

2) Step 2 (Generation of Cable Arrangements): All possible cable arrangements between the base and platform geometry types defined in Step 1 are generated. The only information needed is the number of distinct points of these geometry types, as well as the potential symmetry properties.

Let us consider the n_b distinct points of a given base geometry type, and the n_p distinct points of a platform geometry type. The cable arrangements between these two sets of points can be represented by matrices $\mathbf{A}_S$ of dimension $n_b \times n_p$. The components of $\mathbf{A}_S$ are such that $\mathbf{A}_{S_{i,j}} = 1$, if point i of the base geometry type is connected to point j of the platform geometry type and $\mathbf{A}_{S_{i,j}} = 0$, otherwise. Moreover, in order to generate valid cable arrangements, the two following rules must also be respected.

1) All base points must be used. The sum of the components in each row of $\mathbf{A}_S$ must not be zero.
2) All platform points must be used. The sum of the components in each column of $\mathbf{A}_S$ must not be zero.

In this step, all such matrices $\mathbf{A}_S$ are generated. For instance, when $n = n_b = n_p = 8$, the total number of matrices $\mathbf{A}_S$ is $8! = 40\,320$.

Symmetry properties can also be reflected in the generation of cable arrangements. In this paper, as introduced in Section III-A1, point i of a base (resp. platform) geometry type has a symmetrical point. Let the latter be numbered $n_b - i + 1$ (resp. $n_p - i + 1$). Then, in order to reflect this symmetry into the cable arrangements, we only keep the matrices $\mathbf{A}_S$ such that if $\mathbf{A}_{S_{i,j}} = 1$, then $\mathbf{A}_{S_{n_b-i+1,n_p-j+1}} = 1$. For example, in the case $n = n_b = n_p = 8$, the number of symmetric valid cable arrangements is equal to 384.

3) Step 3 (Generation of Cable-Driven Parallel Robot Geometries): One cable-driven parallel robot geometry is obtained for each possible combination of the following three elements.

1) A base geometry type and values of its dimensional parameters chosen among the discrete set of values defined in Step 1.
2) A platform geometry type and values of its dimensional parameters taken among the discrete set of values defined in Step 1.
3) A cable arrangement between these base and platform geometries taken among the arrangement set generated in Step 2.

Each such combination defines a *cable-driven parallel robot geometry* consisting of the cable drawing point positions in the fixed reference frame, the cable attachment point positions in the platform local frame, and the cable arrangement between these two point sets.

4) Step 4 (Performance Evaluation and Collision Detection): All the cable-driven parallel robot geometries generated in Step 3 are considered in turn. For each one of them, at each pose of the discretized prescribed workspace defined in Step 1, the absence of cable–cable collisions is tested and the value of $r_{\max}$ [see (15)] is computed. The *performance index* of the geometry at hand is defined as the minimum value of $r_{\max}$ over all the poses of the discretized prescribed workspace. Among the cable-driven parallel robot geometries having no collision between the cables, the geometry having the largest performance index is considered to be the best one. The cables being assumed to be straight line segments (cable mass is neglected), the absence of

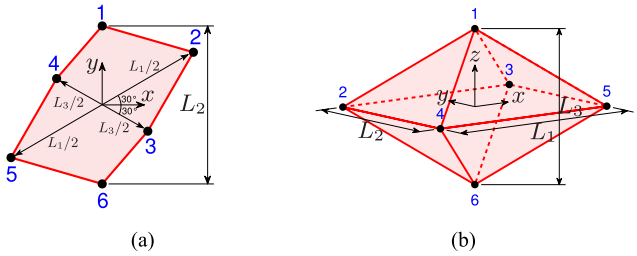

Fig. 7. Two six-point platform geometry types parameterized by L_1, L_2, and L_3. (a) Planar platform. (b) Spatial platform.

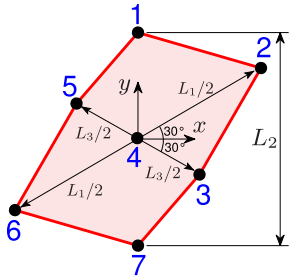

Fig. 8. Seven-point planar platform geometry type parameterized by L_1, L_2, and L_3.

collision between two cables is tested by computing the distance between them [31], [32].

A rough discretization of the prescribed workspace should be used in order to get a reasonable computation time. Consequently, the performances and avoidance of cable–cable collisions should be ascertained at the end of the geometry selection procedure (after the second phase as described in Section III-B), e.g., by means of a fine discretization or of interval analysis.

B. Phase 2: Optimization

The second phase of the optimal geometry selection methodology is briefly introduced in this section. By formulating a nonlinear optimization problem, we aim at locally refining the best cable-driven parallel robot geometry obtained in the first phase (see Section III-A). The latter robot geometry is, thus, taken as the initial guess of a standard iterative gradient-based optimization algorithm.

1) Problem Formulation: In this paper, optimizing a cable-driven parallel robot geometry consists of *maximizing the maximum acceptable horizontal distance* $r_{\max}$ between the platform geometric center P and the platform and payload CoM C [see (15)] over all the poses of a discretized prescribed workspace. For all these poses, the avoidance of cable–cable collisions is formulated as a set of inequality constraints $\mathbf{k}_{collision} \leq \mathbf{0}$ as specified in Section III-B3. Hence, the maximization problem considered here can be written as

$$\begin{aligned} \text{maximize} \quad & \min_{\substack{i=1,2 \\ j=1,\ldots,N_h N_p}} r_{i,j} \\ \text{subject to} \quad & \mathbf{k}_{\text{collision}} \leq \mathbf{0}, \\ \text{over} \quad & \mathbf{p} \in [\mathbf{p}_{\min}, \mathbf{p}_{\max}] \end{aligned} \tag{17}$$

where $r_{i,j}$ is defined in (16), N_h is the number of inequalities in $\mathbf{Cf} \leq \mathbf{d}$ [see (3)], and N_p is the number of poses in the discretized prescribed workspace. Index j refers here to both the inequalities in $\mathbf{Cf} \leq \mathbf{d}$ and the poses of the discretized prescribed workspace.

The vector $\mathbf{p}$ of optimization variables contains the coordinates of the position vectors $\mathbf{a}_i = [a_{ix}, a_{iy}, a_{iz}]^T$ of the cable drawing points (in the fixed base frame) and the position vectors $\mathbf{b}_i = [b_{ix}, b_{iy}, b_{iz}]^T$ of the cable attachment points (in the mobile platform frame). It also contains an angle ψ_0, which defines an offset of the platform reference orientation about the vertical Z-axis of the base frame. The vectors of bound values $\mathbf{p}_{\min}$ and $\mathbf{p}_{\max}$ report the extreme values of $\mathbf{a}_i$ and $\mathbf{b}_i$, which are computed from user-defined bounds on the dimensional parameters of the base and platform geometry types, as well as the extreme values $-\pi$ and $+\pi$ of ψ_0.

In order to solve problem (17) using standard algorithms, it is written in the following equivalent form:

$$\begin{aligned} \text{minimize} \quad & z \\ \text{subject to} \quad & -\arctan(r_{i,j}) \leq z, \\ & i = 1,2 \ \text{ and } \ j = 1,\ldots,N_h N_p \\ & \mathbf{k}_{\text{collision}} \leq \mathbf{0}, \\ \text{over} \quad & z \in \mathbb{R},\ \mathbf{p} \in [\mathbf{p}_{\min}, \mathbf{p}_{\max}] \end{aligned} \tag{18}$$

where to improve the numerical behavior of the optimization solver, the values of $r_{i,j}$ have been scaled using the arctan function to highlight the smallest values w.r.t. the largest ones. It is a large-scale optimization problem involving $6n + 2$ variables and $2N_h N_p + N_c$ inequality constraints, where N_c is the total number of collision constraints. For instance, the geometry optimization of a eight-cable robot ($n = 8$, $N_h = 2C_8^5 = 112$ [30]) evaluated over 27 positions in a given box (center, eight vertices, 12 midedges, and six midfaces) for two orientation angles around the vertical axis ($N_p = 27 \times 2 = 54$) involves $6 \times 8 + 2 = 50$ variables and $2 \times 112 \times 54 + 1512 = 13\,608$ inequality constraints. The total number $N_c = 1512$ of collision constraints is obtained by multiplying the number of cable pairs by N_p.

2) Derivatives of the Performance Criterion: The use of a gradient-based optimization algorithm requires the computation of the derivatives of $r_{i,j}$ w.r.t. the design variables gathered in vector $\mathbf{p}$. According to (16), this computation amounts to calculate the derivatives of the components of vector $\mathbf{d}$ and matrix $\mathbf{C}$ (namely of d_j, $c_{j_{f_z}}$, $c_{j_{t_x}}$, and $c_{j_{t_y}}$) w.r.t. to $\mathbf{p}$. These components depend on $\mathbf{p}$ via the wrench matrix $\mathbf{W}$. The explicit expression of $\mathbf{W}$ in terms of the design variables $\mathbf{p}$ is well known [9], [28], and the determination of its derivatives w.r.t. to $\mathbf{p}$ is straightforward. Moreover, referring to the hyperplane shifting method outlined in Section II-B, calculating the derivatives of $\mathbf{d}$ and $\mathbf{C}$ w.r.t. $\mathbf{W}$ amounts to computing the derivatives of $\mathbf{c}_I = \text{null}(\mathbf{M}_I)$ w.r.t. $\mathbf{W}$. The latter derivatives can be obtained by two means. The first one consists of considering the singular value decomposition of $\mathbf{M}_I$ and then in following the procedure

proposed in [33]. The second one is to use a determinant-based expression of a nullspace spanning vector [34], and then apply the well-known formula of the derivatives of a determinant.

3) Collision Avoidance Constraints: Each collision avoidance inequality constraint in (18) is based on the computation of the distance between two cables. In this paper, the cables are considered to be straight line segments. The distance between two segments $\mathcal{L}_i$ and $\mathcal{L}_j$ must remain greater than the cable diameter δ_c (a small nonnegative value). Hence, the corresponding collision avoidance constraint is

$$k_{\text{collision}} = \delta_c - \text{dist}\left(\mathcal{L}_i,\, \mathcal{L}_j\right) \leq 0. \tag{19}$$

This scalar constraint has to be fulfilled by all cable pairs in every platform poses of the discretized prescribed workspace. All the resulting constraints are gathered in vector $\mathbf{k}_{\text{collision}}$.

In this paper, the algorithm proposed in [32] has been used to compute the distance between two straight line segments and the derivatives of the collision avoidance constraints computed accordingly.

IV. Geometry Selection of a Large Cable-Suspended Robot

This section reports the application of the two-phase optimal geometry selection methodology presented in Section III to the design of a cable-suspended parallel robot. The obtained geometry is new and provides effective performances across a very large workspace. Based on this result, a large cable-suspended parallel robot has been built in the framework of a research project called CoGiRo [35].

A. Input Data

The cable-suspended parallel robot whose geometry is to be determined has 6-DOF and is driven by eight cables.

1) Workspace Dimensions: The inner volume of the fixed base structure is a box of dimensions 14.81 m $\times$ 10.81 m $\times$ 5.58 m ($l \times w \times h$). The prescribed constant-orientation workspace is defined by a scaling of this box: $2/3$ of the length and $1/2$ of the width and height. Its discretization consists of 27 positions (center, eight vertices, 12 midedges, and six midfaces). The required platform rotations are about the vertical axis only with a limited range of $\pm\pi/12$. To define the discretization of the prescribed workspace, five different angles in the range $\pm\pi/12$ were considered in Step 4 of Section III-A. In the local optimization problem of Section III-B1, the two extreme angles $-\pi/12$ and $+\pi/12$ were used.

2) Platform and Payload Masses and Cable Tensions: The mobile platform mass is $m_{\min} = 40$ kg, whereas the total mass of the platform loaded up with the heaviest payload is $m_{\max} = 200$ kg.

The cables are antirotation steel cables of diameter 4 mm. According to the breaking loads of various mechanical parts, the maximum admissible cable tension $\tau_{\max}$ is 5825 N (50% of the cable breaking load). A small positive value should be chosen for $\tau_{\min}$ to restrict cable sagging. In this paper, $\tau_{\min} =$ 20 N has been selected.

3) Base Geometries: A unique fixed base geometry type is considered. It is enclosed in the inner volume of the fixed base structure so that its dimensional parameters L, l, and h, shown in Fig. 4, are set to 14.81, 10.81, and 5.58 m, respectively. It consists of eight drawing points all located at the top as illustrated in Fig. 4. The relative positions between these eight points are defined by distances ΔL and Δl. Due to manufacturing constraints, ΔL and Δl must both be comprised between 255 and 425 mm. In phase 1 (see Section III-A), all acceptable combinations of these bounding values were considered. In phase 2 (see Section III-B), ΔL and Δl were left free between these bounding values.

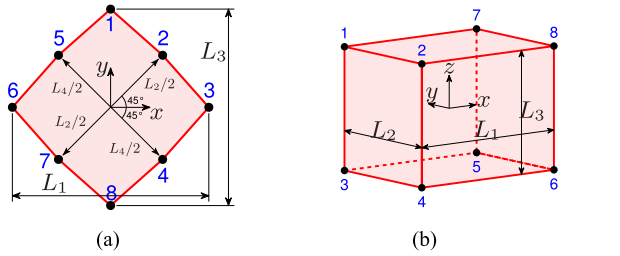

Fig. 9. Two eight-point platform geometry types parameterized by L_1, L_2, L_3 (and L_4). (a) Planar platform. (b) Spatial platform.

4) Mobile Platform Geometries: We constrained the cable attachment points to be enclosed in a cube of side length 1 m. The considered platform geometry types are shown in Figs. 5–9, where two to four parameters L_1 to L_4 are required depending on the geometry type at hand. In the first phase of the geometry selection procedure (see Section III-A), a discrete set of four values included in the interval $[0.25,\ 1]$ (m) was considered for each parameter. The attachment point positions were left free within the 1-m side cube in the second phase (see Section III-B).

B. Optimal Geometry Selection Results

In the first phase (see Section III-A), 1888 cable arrangements were generated, leading to 686 080 different cable-suspended robot geometries. The corresponding performance evaluation and cable–cable collision detection took 3.8 h on a desktop computer (2.53 GHz, 3 Gb of RAM). The best geometry obtained is depicted in Fig. 10(a) and defined in Table I. Only the coordinates of points 1–4 are given, since points 5–8 are symmetrical according to the rule specified in Section III-A. The platform geometry has eight different attachment points located at the vertices of a parallelepiped. It comes from the spatial eight-point geometry type shown in Fig. 9.

The computation time of the second phase (see Section III-B) was 25 min on the same computer (2.53 GHz processor). The resulting optimized geometry is shown in Fig. 10(b) and defined in Table II. Compared with the result of phase 1, it can be observed that the platform geometry is not a parallelepiped anymore and that the orientation offset ψ_0 about the vertical axis is not negligible. The optimization significantly improved the performance index $r_{\max}$ from 16.4 to 28 cm. Such a value of the maximum acceptable horizontal distance between the platform geometric center and platform and payload CoM provides a certain robustness in handling heavy payloads.

In the framework of a research project called CoGiRo [35], the novel geometry shown in Fig. 10(b) has been used to build a large

TABLE I
BASE DRAWING POINT AND PLATFORM ATTACHMENT POINT COORDINATES OBTAINED AFTER PHASE 1 (IN METERS)

		$r_{max} = 16.4$ cm, $\psi_0 = 0°$			
		1	2	3	4
Base	x	−7.15	7.15	−7.41	7.41
	y	5.405	5.405	5.15	5.15
	z	5.576	5.576	5.576	5.576
Platform	x	0.375	−0.375	−0.375	0.375
	y	0.5	0.5	−0.5	−0.5
	z	0.5	−0.5	−0.5	0.5

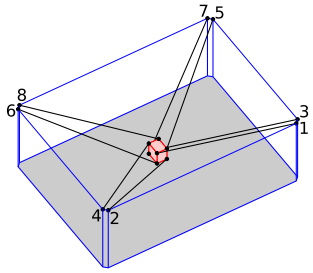

(a)

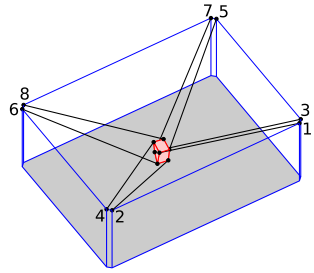

(b)

Fig. 10. Results of the geometry selection methodology. (a) Best cable-suspended robot geometry determined by the first phase (see Section III-A). (b) Optimal geometry obtained in the second phase (see Section III-B).

cable-suspended robot. This geometry yields characteristics that largely outperform the initial requirements given in Section IV-A. Indeed, the prescribed constant orientation workspace was specified as $2/3$ of the length and $1/2$ of the width and height of the fixed base inner volume, which represents 16.6 % of this volume. The actual constant-orientation static workspace (set of feasible static equilibria) for the platform reference orientation and for $m = 100$ kg, $\tau_{\max} = 5825$ N, and $\tau_{\min} = 0$ N occupies 77% of the volume, where m denotes the sum of the mobile platform and payload masses. The projection on soil of this static workspace spans 78% of the robot total footprint. Only small rotations about the vertical axis were initially required. The actual mobile platform orientation capabilities are much better. For instance, at 2 m above the ground in the middle of the workspace, the total orientation range about the vertical axis Z is $105°$ ($-70°$ to $+35°$) and the orientation ranges about the horizontal X and Y axes are both of $\pm 40°$ (taking into account

TABLE II
BASE DRAWING POINT AND PLATFORM ATTACHMENT POINT COORDINATES OBTAINED AFTER PHASE 2 (IN METERS)

		$r_{max} = 28$ cm, $\psi_0 = -8.97°$			
		1	2	3	4
Base	x	−7.15	7.15	−7.41	7.41
	y	5.405	5.405	5.15	5.15
	z	5.576	5.566	5.566	5.576
Platform	x	0.356	−0.266	−0.5	0.341
	y	0.492	0.5	−0.5	−0.5
	z	0.5	−0.5	−0.5	0.5

Fig. 11. Large cable-suspended parallel robot of the project CoGiRo [35]—Robot overall dimensions 15 m × 11 m × 6 m ($L \times l \times h$).

cable collisions with the actual cube-shaped mobile platform, as shown in Fig. 11). With appropriate cable tension distributions, the mechanical design allows the robot to lift masses up to $m =$ 300 kg across 77% of the footprint and 75% of the robot overall volume and up to $m = 500$ kg across 76% of the footprint and 70% of the robot overall volume.

V. CONCLUSION

This paper presented the geometry selection of a large redundantly actuated cable-suspended parallel robot. Based on a particular wrench-feasibility analysis, an original performance index was defined as the maximum acceptable horizontal distance between the mobile platform reference point and the platform and payload CoM. It is of particular interest in applications involving heavy payload manipulations over large workspaces. Used within a two-phase geometry selection strategy, it yielded a new and efficient geometry for 6-DOF cable-suspended robots driven by eight cables. The main merit of this geometry is a very large workspace to footprint ratio. Based on this result, a large 6-DOF cable-suspended robot was built. Its performances demonstrate the relevance of redundant actuation for cable-suspended parallel robots and of the particular robot geometry disclosed in this paper.

A quasi-static modeling was used in this paper since static forces and moments were considered to be predominant. Moreover, the cable mass was neglected. The extension to cases in which the mobile platform dynamics and the cable mass have to be taken into account is a part of our ongoing work.

APPENDIX
PROOFS OF (13) AND (14)

Let us first consider the case of the upper disc $\mathcal{U}$ defined in (12). AW being a convex set, $\mathcal{U} \subseteq$ AW, if and only if (iff) the bounding circle $\mathcal{C}_\mathcal{U}$ of $\mathcal{U}$ is entirely contained in AW, i.e., $\mathcal{C}_\mathcal{U} \subseteq$ AW. The wrenches $\mathbf{f} = [f_x, f_y, f_z, t_x, t_y, t_z]^T$ belonging to $\mathcal{C}_\mathcal{U}$ are such that

$$f_x = f_y = t_z = 0,\ f_z = m_{\max} g, t_x = m_{\max} g r \cos(\alpha),$$
$$t_y = m_{\max} g r \sin(\alpha),\ -\pi < \alpha \leq \pi. \tag{20}$$

According to (3), $\mathcal{C}_\mathcal{U} \subseteq$ AW, iff all the wrenches in (20) satisfy all the inequalities in $\mathbf{Cf} \leq \mathbf{d}$. Let us first consider the jth inequality alone

$$\mathbf{c}_j^T \mathbf{f} \leq d_j. \tag{21}$$

With the notations in (8) and according to (20), all the wrenches of $\mathcal{C}_\mathcal{U}$ verify this inequality iff

$$c_{j_{f_z}} + c_{j_{t_x}} r \cos(\alpha) + c_{j_{t_y}} r \sin(\alpha) \leq \frac{d_j}{m_{\max} g} \quad \forall \alpha \in]-\pi, \pi] \tag{22}$$

which is equivalent to

$$r(c_{j_{t_x}} \cos(\alpha) + c_{j_{t_y}} \sin(\alpha)) \leq \frac{d_j}{m_{\max} g} - c_{j_{f_z}} \quad \forall \alpha \in]-\pi, \pi]. \tag{23}$$

The left-hand side of the latter inequality is a function of α which reaches its maximum when

$$\sin(\alpha) = c_{j_{t_y}} / \sqrt{c_{j_{t_x}}^2 + c_{j_{t_y}}^2} \tag{24}$$

$$\cos(\alpha) = c_{j_{t_x}} / \sqrt{c_{j_{t_x}}^2 + c_{j_{t_y}}^2}. \tag{25}$$

Consequently, (23) is true iff

$$r\sqrt{c_{j_{t_x}}^2 + c_{j_{t_y}}^2} \leq \frac{d_j}{m_{\max} g} - c_{j_{f_z}} \iff r \leq \frac{\frac{d_j}{m_{\max} g} - c_{j_{f_z}}}{\sqrt{c_{j_{t_x}}^2 + c_{j_{t_y}}^2}}. \tag{26}$$

It follows directly from (26) that the maximum value $r_{1,j}$ of r such that all the wrenches of $\mathcal{C}_\mathcal{U}$ verify the jth inequality (21) is equal to

$$r_{1,j} = \frac{\frac{d_j}{m_{\max} g} - c_{j_{f_z}}}{\sqrt{c_{j_{t_x}}^2 + c_{j_{t_y}}^2}}. \tag{27}$$

Hence, the maximum value r_1 of r such that all the wrenches belonging to $\mathcal{C}_\mathcal{U}$ satisfy all the inequalities in $\mathbf{Cf} \leq \mathbf{d}$, i.e., such that $\mathcal{C}_\mathcal{U} \subseteq$ AW, is equal to

$$r_1 = \min_j r_{1,j} = \min_j \frac{\frac{d_j}{m_{\max} g} - c_{j_{f_z}}}{\sqrt{c_{j_{t_x}}^2 + c_{j_{t_y}}^2}}. \tag{28}$$

Finally, as stated at the beginning of this appendix, $\mathcal{U} \subseteq$ AW, iff $\mathcal{C}_\mathcal{U} \subseteq$ AW so that (13) is proved, i.e., the maximum value r_1 of r such that the upper disc $\mathcal{U}$ of RW is fully included in AW is given by (28).

The proof of (14) is exactly similar to the one proposed above for (13) with $m_{\min}$ in place of $m_{\max}$.

REFERENCES

[1] J. Albus, R. Bostelman, and N. Dagalakis, "The NIST ROBOCRANE," *J. Robot. Syst.*, vol. 10, no. 5, pp. 709–724, 1993.

[2] S. Kawamura, W. Choe, S. Tanaka, and S. R. Pandian, "Development of an ultrahigh speed robot falcon using wire drive system," in *Proc. IEEE Int. Conf. Robot. Autom.*, Nagoya, Japan, 1995, pp. 215–220.

[3] M. Carricato and J.-P. Merlet, "Stability analysis of underconstrained cable-driven parallel robots," *IEEE Trans. Robot.*, vol. 29, no. 1, pp. 288–296, Feb. 2013.

[4] G. Rosati, D. Zanotto, and S. K. Agrawal, "On the design of adaptive cable-driven systems," *ASME J. Mech. Robot.*, vol. 3, pp. 1–13, May 2011.

[5] X. Zhou, C. P. Tang, and V. Krovi, "Analysis framework for cooperating mobile cable robots," in *Proc. IEEE Int. Conf. Robot. Autom.*, Saint Paul, MN, USA, 2012, pp. 3128–3133.

[6] P. Gallina and G. Rosati, "Manipulability of a planar wire driven haptic device," *Mech. Mach. Theory*, vol. 37, no. 2, pp. 215–228, Feb. 2002.

[7] R. L. Williams II, B. Snyder, J. S. Albus, and R. V. Bostelman, "Seven-dof cable-suspended robot with independent metrology," in *Proc. ASME Design Eng. Tech. Conf. Comput. Inform. Eng. Conf.*, Paper DETC2004/MECH-57125 [CD-ROM], Salt Lake City, UT, USA, Sep. 2004, pp. 317–325.

[8] C. Ferraresi, M. Paoloni, S. Pastorelli, and F. Pescarmona, "A new 6-dof parallel robotic structure actuated by wires: The wiro-6.3," *J. Robot. Syst.*, vol. 21, no. 11, pp. 581–595, 2004.

[9] M. Hiller, S. Fang, S. Mielczarek, R. Verhoeven, and D. Franitza, "Design, analysis and realization of tendon-based parallel manipulators," *Mech. Mach. Theory*, vol. 40, no. 4, pp. 429–445, Apr. 2005.

[10] R. L. Williams II, M. Xin, and P. Bosscher, "Contour-crafting-cartesian-cable robot system concepts: Workspace and stiffness comparisons," presented at the ASME Int. Design Engineering Technical Conf. Comput. Information Engineering Conf., Brooklyn, NY, USA, Aug. 2008, Paper DETC2008-49478 [CD-ROM].

[11] M. M. Aref and H. D. Taghirad, "Geometrical workspace analysis of a cable-driven redundant parallel manipulator: KNTU CDRPM," in *Proc. IEEE/RSJ Int. Conf. Intell. Robots Syst.*, Nice, France, 2008, pp. 1958–1963.

[12] Y. Takeda and H. Funabashi, "Kinematic synthesis of spatial in-parallel wire-driven mechanism with six degrees of freedom with high force transmissibility," presented at the ASME Design Engineering Technical Conf. Comput. Information Engineering Conf., Baltimore, MD, USA, 2000, Paper DETC2000/MECH-14090.

[13] S. Perreault and C. M. Gosselin, "Cable-driven parallel mechanisms: Application to a locomotion interface," *ASME J. Mech. Des.*, vol. 130, no. 10, pp. 1–8, Oct. 2008.

[14] T. Bruckmann, L. Mikelsons, T. Brandt, M. Hiller, and D. Schramm, "Design approaches for wire robots," presented at the ASME Int. Design Engineering Technical Conf. Comput. Information Engineering Conf., San Diego, CA, USA, Sep. 2009, Paper DETC2009-86720 [CD-ROM].

[15] K. Azizian and P. Cardou, "The dimensional synthesis of planar parallel cable-driven mechanisms through convex relaxations," *ASME J. Mech. Robot.*, vol. 4, no. 3, pp. 1–13, Aug. 2012.

[16] I. Ebert-Uphoff and P. A. Voglewede, "On the connections between cable-driven robots, parallel manipulators and grasping," in *Proc. IEEE Int. Conf. Robot. Autom.*, New Orleans, LA, USA, 2004, pp. 4521–4526.

[17] P. Lafourcade, M. Llibre, and C. Reboulet, "Design of a parallel wire-driven manipulator for wind tunnels," in *Proc. Workshop Fundam. Issues Future Res. Directions Parallel Mech. Manipulators*, Quebec City, Canada, 2002, pp. 187–194.

[18] A. Pott, H. Mutherich, W. Kraus, V. Schmidt, P. Miermeister, and A. Verl, "IPAnema: A family of cable-driven parallel robots for industrial applications," in *Cable-Driven Parallel Robots*, T. Bruckmann and A. Pott, Eds. New York, NY, USA: Springer-Verlag, 2013, pp. 119–134.

[19] S. Tadokoro, S. Nishioka, T. Kimura, M. Hattori, T. Takamori, and K. Maeda, "On fundamental design of wire configurations of wire-driven parallel manipulators with redundancy," in *Proc. Japan/USA Symp. Flexible Autom.*, Boston, MA, USA, 1996, pp. 151–158.

[20] H. Khakpour, L. Birglen, and S.-A. Tahan, "Synthesis of differentially driven planar cable parallel manipulators," *IEEE Trans. Robot.*, vol. 30, no. 3, pp. 619–630, Jun. 2014.

[21] J. Pusey, A. Fattah, S. Agrawal, and E. Messina, "Design and workspace analysis of a 6-6 cable-suspended parallel robot," *Mech. Mach. Theory*, vol. 39, pp. 761–778, 2004.

[22] X. Tang and R. Yao, "Dimensional design of the six-cable driven parallel manipulator of FAST," *ASME J. Mech. Des.*, vol. 133, no. 11, pp. 1–12, Nov. 2011.

[23] J.-D. Deschenes, P. Lambert, S. Perreault, N. Martel-Brisson, N. Zoso, A. Zaccarin, P. Hebert, S. Bouchard, and C. Gosselin, "A cable-driven parallel mechanism for capturing object appearance from multiple

viewpoints," presented at the 6th Int. Conf. 3-D Digital Imaging Modeling, Montreal, QC, Canada, 2007.
[24] P. Bosscher, A. T. Riechel, and I. Ebert-Uphoff, "Wrench-feasible workspace generation for cable-driven robots," *IEEE Trans. Robot.*, vol. 22, no. 5, pp. 890–902, Oct. 2006.
[25] S. Bouchard, C. M. Gosselin, and B. Moore, "On the ability of a cable-driven robot to generate a prescribed set of wrenches," *ASME J. Mech. Robot.*, vol. 2, no. 1, pp. 1–10, 2010.
[26] S. Abdelaziz, L. Esteveny, L. Barbé, P. Renaud, B. Bayle, and M. de Mathelin, "Development of a mr-compatible cable-driven manipulator: design and technological issues," in *Proc. IEEE Int. Conf. Robot. Autom.*, Saint Paul, MN, USA, 2012, pp. 1488–1494.
[27] A. Taghavi, S. Behzadipour, N. Khalilinasab, and H. Zohoor, "Workspace improvement of two-link cable-driven mechanisms with spring cable," in *Cable-Driven Parallel Robots*, T. Bruckmann and A. Pott, Eds. New York, NY, USA: Springer, 2013, pp. 201–213.
[28] R. G. Roberts, T. Graham, and T. Lippitt, "On the inverse kinematics, statics, and fault tolerance of cable-suspended robots," *J. Robot. Syst.*, vol. 15, no. 10, pp. 581–597, 1998.
[29] G. M. Ziegler, *Lectures on Polytopes* (Graduate Texts in Mathematics 152). New York, NY, USA: Springer-Verlag, 1994.
[30] M. Gouttefarde and S. Krut, "Characterization of parallel manipulator available wrench set facets," in *Advances in Robot Kinematics*, J. Lenarcčicč and M. M. Stanisčić, Eds. New York, NY, USA: Springer-Verlag, 2010, pp. 475–482.
[31] V. Lumelsky, "On fast computations of distance between line segments," *Inform. Process. Lett.*, vol. 21, no. 2, pp. 55–61, Aug. 1985.
[32] C. Ericson, *Real-Time Collision Detection* (Series in Interactive 3-D Technology). San Mateo, CA, USA: Morgan Kaufmann, Jan. 2005.
[33] T. Papadopoulo and M. Lourakis, "Estimating the jacobian of the singular value decomposition: Theory and applications," in *Proc. Eur. Conf. Comput. Vision*, Dublin, Ireland, Jun. 2000, pp. 554–570.
[34] M. Gouttefarde and C. M. Gosselin, "On the properties and the determination of the wrench-closure workspace of planar parallel cable-driven mechanisms," in *Proc. ASME Design Eng. Tech. Conf. Comput. Inform. Eng. Conf.*, Paper DETC2004/MECH-57127 [CD-ROM], Salt Lake City, UT, USA, Sep. 2004, pp. 337–346.
[35] (2013). Website of project CoGiRo [Online]. Available: http://www.lirmm.fr/cogiro/